Effects of deformation on the electronic structure of a single-walled carbon nanotube bundle

Dong Chen,[1,2] Taizo Sasaki,[1] Jie Tang,[3] and Lu-Chang Qin[4]
[1]*Computational Materials Science Center, National Institute for Materials Science, Tsukuba 305-0047, Japan*
[2]*Shenyang National Laboratory for Materials Science, Institute of Metal Research, Chinese Academy of Sciences, Shenyang 110016, People's Republic of China*
[3]*1D Nanomaterials Research Group, National Institute for Materials Science, Tsukuba 305-0047, Japan*
[4]*W.M. Keck Laboratory for Atomic Imaging and Manipulation, Department of Physics and Astronomy and Curriculum in Applied and Materials Sciences, University of North Carolina at Chapel Hill, Chapel Hill, North Carolina 27599-3255, USA*
(Received 11 September 2007; revised manuscript received 17 December 2007; published 13 March 2008)

We have studied the effects of uniaxial pressure on the geometric structure and the electronic structure of single-walled carbon nanotube bundles theoretically. The local-density approximation in the density-functional theory has been applied to three types of carbon nanotube bundles, made up of the (8, 0), (10, 0), and (11, 0) tubes under uniaxial pressure perpendicular to the tubule axis. In all these types of bundles, an abrupt change is observed in the deformation of the tubes and their configuration at a certain pressure. It is also found that, despite a similar change of the lattice constants of the bundle, the deformation and the configuration of the tubes depend strongly on their types: While the (8, 0) tube bundle has a dense structure at high pressures, larger tube bundles prefer a loose one. All types of bundles, which are calculated to be semiconducting, exhibit a semiconductor-metal transition before or at the beginning of the abrupt change of the lattice constants when they are deformed by the uniaxial pressure. The pressure effect on the energy gap, however, is not monotonous: a decrease and an upturn followed by its disappearance. By analyzing the atomic arrangement, the band structure, and the wave functions of the three types of carbon nanotube bundles, the relationship between them is also established.

DOI: 10.1103/PhysRevB.77.125412 PACS number(s): 73.22.−f, 71.20.−b, 71.30.+h, 71.15.Mb

I. INTRODUCTION

In materials science, the major concerns are about structures, properties, and the relationship between them. Carbon nanotubes[1] have recently attracted much attention because they have the most potential for applications in nanometer-scale electronic devices which exhibit unprecedented physical, chemical, and electrical properties. In addition, the electronic properties of carbon nanotubes are extraordinary and unique. For example, a carbon nanotube can exhibit variations in its electronic structures by many ways. Notable is the fact that a carbon nanotube can be either semiconducting or metallic, depending on its diameter and helicity.[2,3] Modifications of the electronic properties of a carbon nanotube can be carried out by such ways as applying pressure,[4] electric and magnetic fields,[5] chemical treatment,[6] etc.

A detailed understanding of the electronic properties of single-walled carbon nanotubes (SWCNTs) is important for their applications. Recently, many experimental and theoretical studies[4,7–17] revealed the structural and mechanical behaviors of bundles of SWCNTs under external pressure. The electronic properties of a SWCNT bundle under pressure, however, have received much less attention while most of the previous studies were only on the isolated carbon nanotubes.[11–13,17–22] The behavior of a bundle during deformation is expected to be very different from that of the isolated tubes since the intertubular interactions will affect the electronic properties. Moreover, the deformation of a bundle occurs not only in the shape of the tube but also in the configuration of the tubes. Therefore, it is very important to give an accurate description of the nature of the electronic structure of the deformed SWCNT bundles.

Previous studies suggested elliptical deformation in the structural changes under pressure.[16,17,23–25] In our study, special attention is paid to this type of deformation for several reasons. The current understanding is that the circular nanotube cross section is distorted to an elliptic geometry under hydrostatic pressure.[7] In Ref. 4, it was reported that the semiconducting SWCNTs exhibited a change of energy gap by pressure and it was suggested that the large change would be induced by the elliptical deformation of the tubes. Furthermore, it was put forward that the elliptical deformation can be induced to the nanotubes by chemical modification and produces changes in the electronic structures.[5] In addition, similar elliptical deformation may also be induced by bending in the nanotubes[26] or when the nanotubes run across obstacles such as other tubes.[27] In such a way, this type of deformation can be seen on many occasions.

In this work, we have studied the effects of deformation on the electronic structures of SWCNT bundles, especially in the semiconducting state. We attempt to address the following: (1) what the characteristics of the bundle under pressure are and (2) how the electronic structure of the bundle changes in the process including the semiconductor-metal transition. Generally, the $(n,0)$ zigzag nanotubes are semiconducting and are only metallic if n is an integer multiple of three. We chose the (8, 0), (10, 0), and (11, 0) bundles, which are all semiconductors with a narrow energy gap in an isolated form at the ambient condition. For the crystalline bundles of (8, 0), (10, 0), and (11, 0) SWCNTs, we use the local-density approximation (LDA) in the density-functional theory to calculate the geometries and the electronic structures. The deformation of the bundle is induced by a uniaxial pressure applied perpendicular to the tubule axis, as shown

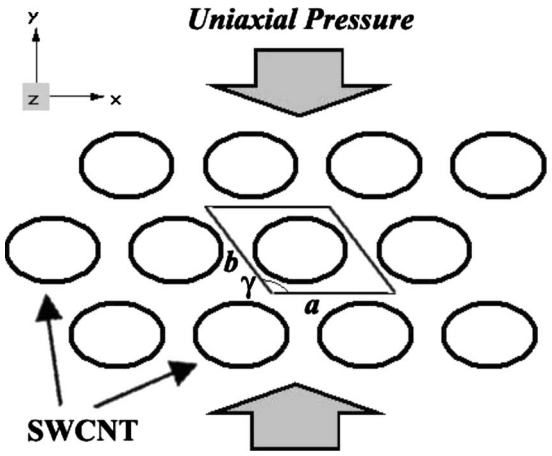

FIG. 1. Uniaxial pressure with the cross section of the bundle.

in Fig 1. These calculations will reveal the change of the structural and the electronic properties of the bundle to the uniaxial pressure theoretically. By analyzing the band structures and the wave functions of the bundles, the changes of the electronic properties will also be discussed.

II. COMPUTATIONAL DETAILS

The first-principles electronic structure calculations have been performed with the pseudopotential formalism[28,29] and the plane-wave basis set within the density-functional theory using the ABINIT code.[30] The exchange-correlation energy is treated with the LDA in the Ceperley-Alder form[31] with the Perdew-Wang parametrization.[32] Even though the LDA has the well known problem of underestimating the energy gap, it is still very useful to capture the most important aspects of the electronic structure. All the calculations have been performed in a self-consistent manner by using the conjugate-gradient algorithm.[33,34] The structure has been optimized by making the Hellmann-Feynman forces smaller than 10^{-2} eV/Å on each atom. A cutoff energy of 408 eV (15 hartree) for the plane-wave basis set has been found to be sufficient to achieve the convergence of 10^{-5} hartree/atom in the total energy by comparing the results with higher cutoff energies up to 952 eV (35 hartree). The Brillouin zone integration was done on the $2\times2\times4$ Monkhorst-Pack grid points.[35] After the structural optimization with these numerical settings, the detailed band structures were obtained.

All the carbon nanotube bundle structures were constructed from one individual tube placed in a hexagonal unit cell with the lattice constants of a, b, c, and γ (Fig. 1). There are $4n$ carbon atoms in the unit cell for the $(n,0)$ SWCNT. The lattice constants a and b are lying in the circular cross section of the tube and the lattice constant c is taken along the tube axis. The cross section is within the xy plane and the tube axis is along the z direction. The lattice constants and the atomic positions in the unit cell were relaxed without any constraint on the lattice symmetry except the three-dimensional translational one. The deformation of the bundle was generated by a uniaxial pressure. The compressive pressure is applied along the y axis in the xy plane so as to shorten the diameter in the y direction. The structural deformation may proceed stepwise under different pressures, and the initial geometry at each pressure was taken from the optimized structure at the previous step.

To give a feasibility evidence of the computational method, the energy gap of the isolated (8, 0), (10, 0), and (11, 0) SWCNTs was calculated. The band structure calculations were performed after the geometry optimization in terms of the supercell geometry with the closest intertubular spacing of more than 9 Å, which is large enough to neglect the interactions between the nanotubes. Table I lists the energy gaps E_{gap} calculated in this study and compares them with the previous computational results. In this table, it is clearly shown that our results are in good agreement with other theoretical values. These give us a reasonable basis to perform the theoretical research on the nanotube bundles.

Then, the same method was applied to the (8, 0), (10, 0), and (11, 0) SWCNT bundles, and each energy gap under the ambient condition was obtained as 0.129, 0.172, and 0.429 eV, respectively. It can be seen that the energy gap in each bundle becomes smaller than that of the corresponding isolated SWCNT. This fact indicates that the intertubular interaction will reduce the energy gap significantly. Reich *et al.*[36] obtained the metallic electronic structure for the (10, 0) bundle. We will discuss this discrepancy later.

III. RESULTS AND DISCUSSION

A. Geometric and electronic structures of (8, 0) and (11, 0) bundles

For the (8, 0) bundle, the calculation results on the lattice constants, the angle γ, and the energy gap are shown as a

TABLE I. Calculated energy gap E_{gap} of isolated (8, 0), (10, 0), and (11, 0) single-walled carbon nanotubes with D being the diameter of the $(n,0)$ zigzag nanotubes.

		E_{gap} (eV)					
$(n,0)$	D (Å)	This study	Ref. 18	Ref. 19	Ref. 20	Ref. 21	Ref. 22
(8,0)	6.26	0.508	0.643	0.730	0.590	0.570	0.500
(10, 0)	7.83	0.848	0.764	0.880	0.770	0.910	
(11, 0)	8.61	0.904	0.939	1.130	0.930	0.770	

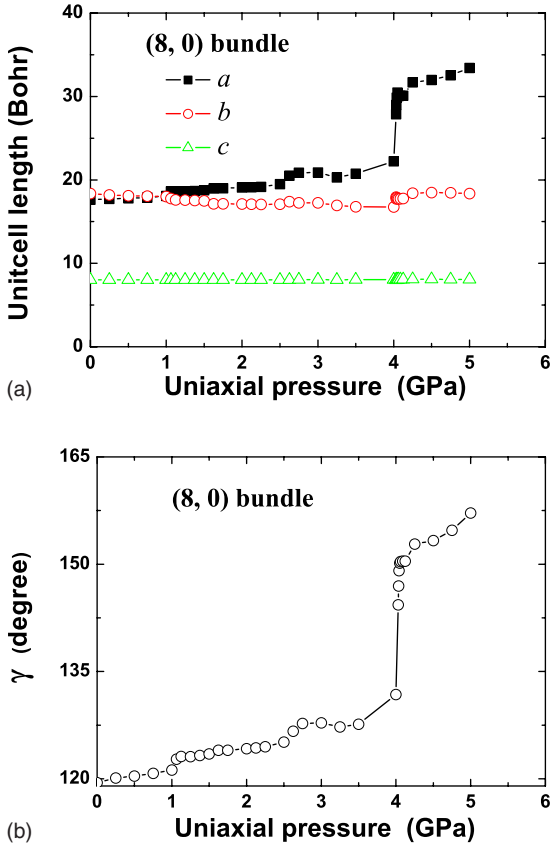

FIG. 2. (Color online) Variations of (a) lattice constants and (b) angle γ with pressure in the (8, 0) carbon nanotube bundle.

function of pressure in Figs. 2 and 3, where γ is the angle between the a and b axes of the unit cell. At zero pressure, the lattice constant a is slightly smaller than b because of the incommensurate symmetry of each tube with the hexagonal lattice. With a pressure increase, a and b are approaching each other, they become almost same at 1.0 GPa, and the energy gap shows a rapid decrease to 0.75 GPa followed by a small upturn. At 1.125 GPa, the energy gap vanishes and the (8,0) bundle becomes metallic. After the semiconductor-metal transition, the lattice constant a becomes larger and the

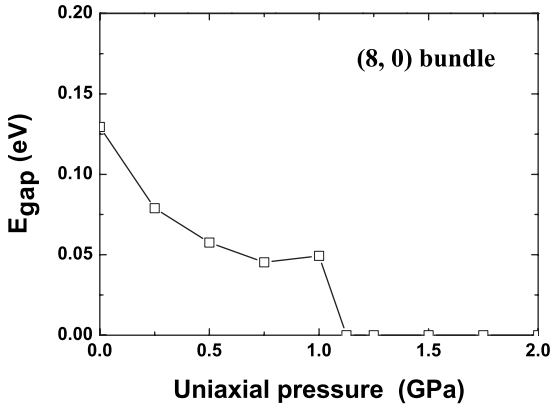

FIG. 3. Variation of the energy gap with pressure in the (8, 0) carbon nanotube bundle.

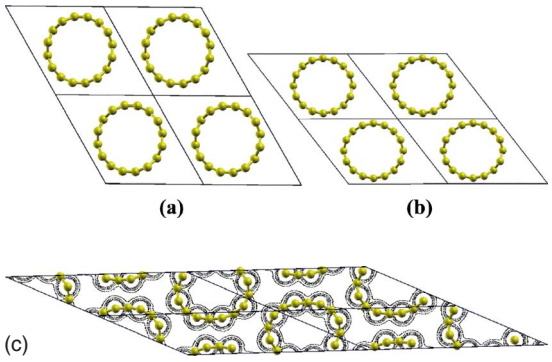

FIG. 4. (Color online) Schematic view of the cross section of the (8, 0) bundle at (a) 0 GPa (a=17.6 bohr, b=18.3 bohr, e'=0.23), (b) 3.0 GPa (a=20.9 bohr, b=17.2 bohr, e'=0.34), and (c) 5.0 GPa (a=33.4 bohr, b=18.4 bohr, e'=0.67). Contour plot of the electron density distribution is also illustrated in (c). All contour lines are in the range of 0–0.05 e/bohr^3. The gray spheres (yellow online) represent carbon atoms.

difference between a and b gradually increases with pressure. The angle γ and the lattice constant a exhibit noticeable changes at 1.125, 2.75, and 4.0 GPa. It seems that the closure of the energy gap has a close relation with the change of the angle γ at 1.125 GPa. At about 4.0 GPa, a larger increase suddenly occurs to the lattice constant a and the angle γ. The rapid increase of a suggests that the cross section of the carbon nanotube becomes more elliptic. In contrast, the lattice constant c does not show any obvious change at the whole pressure range studied.

Figure 4 illustrates the shape of the cross section of the (8, 0) bundle at pressures of 0, 3.0, and 5.0 GPa. It can be seen that the changes of the lattice constants are not only due to the change of the arrangement of the tube but also to that of the cross section. The eccentricities e' (see the Appendix for details) were estimated to be 0.23, 0.34, and 0.67 at each pressure. It should be noted that e' at zero pressure is not zero and the major axis is along the y direction. Such a spontaneous deformation makes the difference in the lattice constants described above.

While a rapid change of the lattice parameters occurs at 4.0 GPa, the metallization pressure is between 1.0 and 1.25 GPa. Thus, large deformation of the bundle is not necessary for the semiconductor-metal transition to occur. However, a discontinuous change of the lattice parameters can be seen in the pressure range where an abrupt decrease of the energy gap occurs. Therefore, the metallization of the (8, 0) bundle may be due to the change of the structure, especially the angle γ.

Figures 5 and 6 show the calculated pressure dependence of the lattice constants, the angle γ, and the energy gap of the (11, 0) bundle. This type of carbon nanotube bundle also has three characteristics in the whole pressure range. (1) Semiconducting feature: at zero pressure, the cross section of the tube is slightly deformed. After the initial rapid decrease of the energy gap, it shows a small increase up to 2.5 GPa. Beyond 2.5 GPa, the energy gap decreases again and closes at 3.25 GPa. (2) Metallic character: at 3.25 GPa, the semiconductor-metal transition is observed. (3) Large struc-

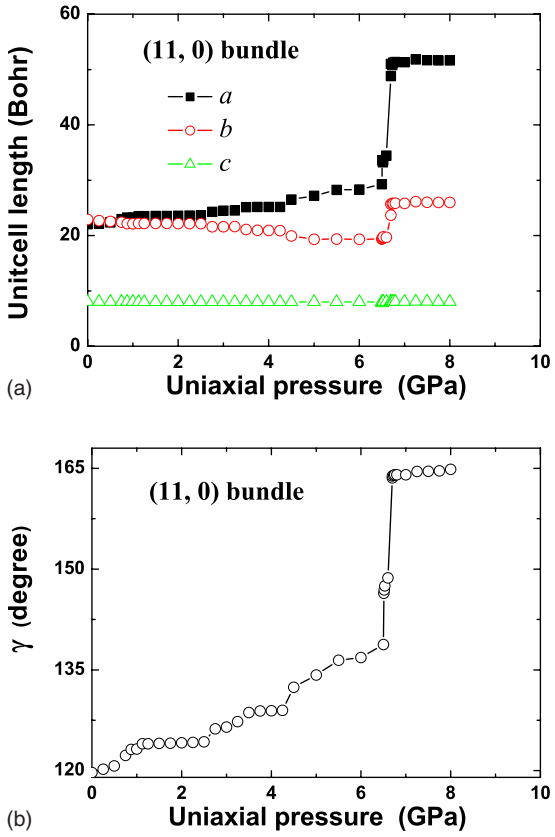

FIG. 5. (Color online) Variations of (a) lattice constants and (b) angle γ with pressure in the (11, 0) carbon nanotube bundle.

tural deformation: Fig. 7 illustrates the geometry of the cross section of the (11, 0) bundle at 0, 5.5, and 6.7 GPa. It can be seen that the tubes with an elliptic geometry change to flat ones. Following a rather smooth variation of a and b and several noticeable jumps of γ, a large structural deformation occurs in the bundle at the pressure of 6.7 GPa.

It should be noted that the disappearance of the energy gap does not imply the occurrence of a large geometric deformation but it closely corresponds to the change of the angle γ at about 3.25 GPa. The metallization of the (11, 0) bundle may be due to the structural change, especially the change of angle γ.

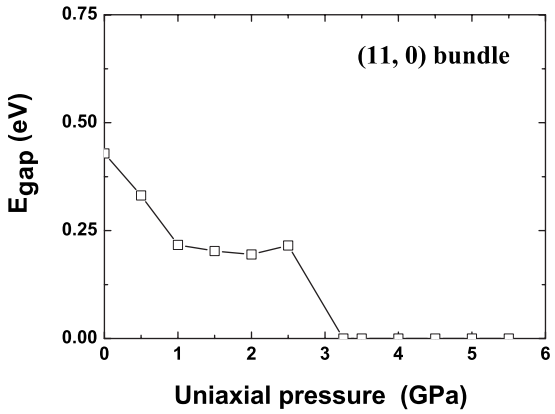

FIG. 6. Variation of energy gap with pressure in the (11, 0) carbon nanotube bundle.

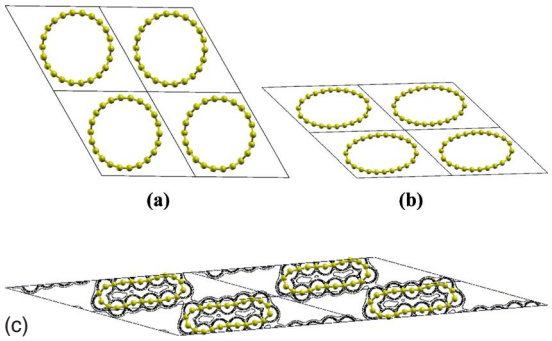

FIG. 7. (Color online) Schematic view of the cross section of the (11, 0) bundle at (a) 0 GPa (a=22.0 bohr, b=22.8 bohr, e'=0.24), (b) 5.5 GPa (a=28.2 bohr, b=19.3 bohr, e'=0.86), and (c) 6.7 GPa (a=48.8 bohr, b=23.6 bohr, e'=0.93). Contour plot of electron density distribution is also illustrated in (c). All contour lines are in the range of 0–0.03 e/bohr^3. The gray spheres (yellow online) represent carbon atoms.

The behavior similar to the (8, 0) bundle can be seen in the change of the lattice constants and the energy gap: a steep decrease of the energy gap at the metallization pressure and a sudden change of the lattice constants at a higher pressure.

In spite of the similarity, however, there are some differences in the atomistic geometry and the configuration of the tubes in the (8, 0) and (11, 0) bundles under deformation. While the former bundle has a close-packed arrangement of the elliptic tubes, as shown in Fig. 4(c), the latter exhibits a loose configuration with the peanut-shaped tubes. The unit cell of the (8, 0) bundle at 5.0 GPa is lengthened along the x axis and shortened in the y direction. Each tube moves in such a way that it inserts its neighbors along the y axis but the shape of the cross section only exhibits a slightly elliptic deformation. Collapse of the large tubes was not observed. The abrupt increase of the lattice parameters shown in Fig. 2 is due to the change in the configuration of tubes. On the other hand, in the case of the (11, 0) bundle at 6.7 GPa, both the shape of the unit cell and that of the tube cross section change very much, as shown in Fig. 7(c). The collapse of the tube can be observed with a transformation of the tube cross section to a peanut shape. The abrupt increase of the parameter a is due to the change in the configuration of tubes plus the large deformation of the tubes. This is because the larger diameter of the (11, 0) tube makes it more flexible than the (8, 0) tube.[12,37] The deviating of the cross section from the ideal bundle is observed at zero pressure in a similar manner to the (8, 0) bundle.

The electron density distributions for the (8, 0) and (11, 0) bundles are illustrated by the contour plots in Figs. 4(c) and 7(c), respectively. For the (8, 0) bundle, the electrons distribute almost spherically around the carbon atoms. The difference in the distribution of the (11, 0) bundle is the accumulation of electrons between the tubes. The atoms connected by this accumulation are separated by 5.9 bohr, which is almost the same as the nearest-neighbor distance between the

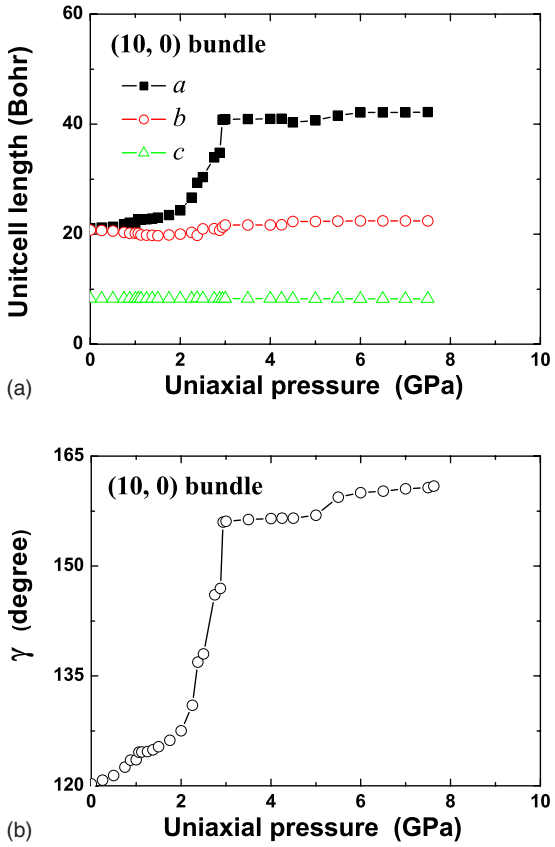

FIG. 8. (Color online) Variations of (a) lattice constants and (b) angle γ with pressure in the (10, 0) carbon nanotube bundle.

(8, 0) tubes shown in Fig. 4(c). For the (11, 0) bundle, the sp^3 orbital in the region of small curvature for each tube makes the covalent bonds with other tubes that are directional, as shown in Fig. 7(c). This is why the geometric configuration in the (11, 0) bundle has a loose packing structure. It indicates that the properties of the (8, 0) and the (11, 0) bundles in the metallic phase might be very different, although their semiconducting properties are similar.

B. Geometric and electronic structures of (10, 0) bundle

The variations of the lattice constants and the angle γ of the (10, 0) bundle with pressure are shown in Fig. 8, and that of the energy gap in Fig. 9. Similar to the previous cases, the lattice parameters vary gradually and an abrupt change occurs in a narrow pressure range at about 2.5 GPa. The cross sections of the bundle are depicted in Fig. 13. It can be seen that the nanotubes retain the elliptic shape under this deformation. Thus, the (10, 0) bundle displays the deformation behavior of the (8, 0) bundle basically. It should be mentioned that the deformation at zero pressure is different to those of the (8, 0) and (11, 0) bundles: the major axes of this case is along the x axis.

On the contrary to the lattice parameters, the energy gap has a different pressure dependence. After the initial decrease, it increases remarkably before metallization. From comparison with the pressure dependence of the lattice parameters, we can see that the energy gap change is closely related to it. Especially, metallization occurs under large deformation. It should be noted that the metallization of the (8, 0) and (11, 0) bundles was observed at a pressure much lower than that for the large deformation.

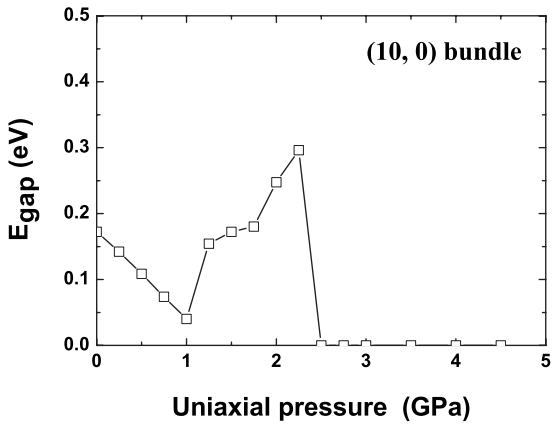

FIG. 9. Variation of energy gap with pressure for the (10, 0) bundle.

C. Band structures

To understand how the electronic properties of the bundle change, we also analyzed the change of the band structures of the carbon nanotube bundle under pressure.

Although the tubes are aligned in a triangular lattice, the symmetry of the bundle is lower than hexagonal even at zero pressure due to a lack of hexagonal symmetry in the nanotube itself. We will use the labels of the points in the Brillouin zone given as depicted in Fig. 10 in the following discussion.

As known in the band structure of a single carbon nanotube, the dispersions are considerably large along the directions parallel to the tube axis, which corresponds to KH, ML, and ΓA lines in Fig. 10. However, it has also been accepted that both the edges of the valence and the conduction bands appear at the point $k_z=0$ for the semiconducting $(n,0)$ tube in isolated form. Thus, in the bundle form, the band structure on the plane $k_z=0$ is considered to be essential. In fact, our calculations have shown that the minimum energy gap always appears on the plane $k_z=0$.

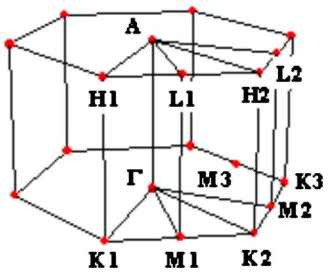

FIG. 10. (Color online) Symmetry points and lines in hexagonal Brillouin zone.

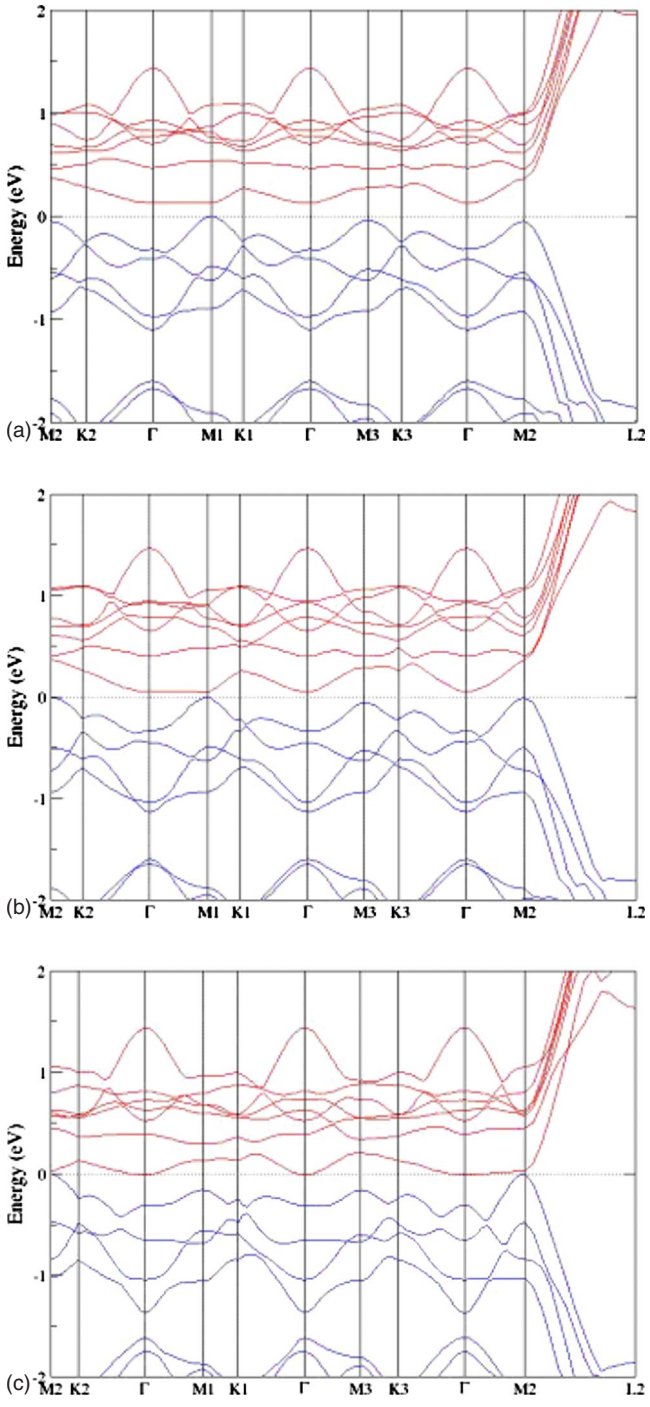

FIG. 11. (Color online) Band structures of the (8, 0) bundle along several symmetry lines under (a) 0 GPa, (b) 1.0 GPa, and (c) 1.125 GPa. The top of the valence band on the Fermi level E_F is set to zero.

Figure 11 shows the band structures of the (8, 0) bundle at (a) 0 GPa, (b) 1.0 Gpa, and (c) 1.25 GPa. At 0 GPa, the top of the valence band can be seen at the M1 point. The lowest conduction band (LCB) has minima at the M1 and Γ points within 0.05 eV. It is difficult to determine whether the energy gap is direct or indirect in the present calculations. It can also be seen that the energy gap at the M2 and M3 points is clearly different from that at M1, which is due to the fact that the symmetry in the Brillouin zone is incommensurate with that of the tube and further confirms that the cross section of the tube is slightly deformed even at 0 GPa.

Under 1.0 GPa pressure, as shown in Fig 11(b), LCB is shifted downward both at M1 and at Γ with respect to the top of the valence band. Up to 1.0 GPa, there is no significant change of the band dispersion. Nevertheless, the position of the top of the valence band becomes unclear by approaching of the levels at M1 and M2. The energy levels at both points are within 0.1 eV. The bottom of the conduction band is at Γ or M1. Also, extra attention should be paid to the fact that the energy gap at the M3 point shows a slight increase with the symmetry lowering.

In the case of Fig. 11(c), both LCB and the highest valence band (HVB) clearly show changes at the M1 point. At the same time, LCB at M2 suddenly drops at 1.125 GPa, LCB has merged with HVB near the M2 point, and they almost coincide with the Fermi level along the ΓM2 line. These changes explain how the energy gap has closed in the band structure. When the pressure exceeds 1.125 GPa, the (8, 0) bundle will exhibit a completely metallic behavior.

After analyzing the band structures, it could reveal some possible mechanisms about the variation of the electronic properties of the bundle up to the semiconductor-metal transition. As a general trend of the band structure variation, the change in amplitude of the conduction band is substantially larger than that of the valence band in the electronic structure. Considering the fact that the uniaxial pressure promotes the symmetry lowering, the electronic states of LCB should be very sensitive to the symmetry of the bundle.

Calculations for the (11, 0) bundle indicated that the change of its band structure due to applied uniaxial pressure share some common features with the (8, 0) bundle. The maxima of HVB can be found at M1, M2, and M3 from 0.0 to 2.5 GPa. The energy levels are within 0.1 eV, and thus the top of the valence band cannot be identified. The bottom of the conduction band is at M1 or M3, and no significant change of dispersion was observed. Metallization between 2.5 and 3.0 GPa occurs by an abrupt drop down at M3 and Γ with respect to the top of the valence band.

The pressure effect on the energy gap of the (10, 0) bundle is rather complicated, as described above. Thus, we analyze the band structure in a different way. According to the calculated results, the change of energy gap is confined by the band structure at the M3 and Γ points for the (10, 0) bundle. Figure 12 shows the relative variations of some LCBs and HVBs at the M3 and Γ points under pressure.

The indirect energy gap of 0.172 eV at 0 GPa comes from the first LCB at M3 and HVB at Γ. From 0 to 1.0 GPa, the first LCB at M3 approaches obviously to HVB at Γ, i.e., the top of the valence band, which results in a decrease in the energy gap. However, at 1.25 GPa, the first LCB at M3 suddenly moves apart from it. At the same time, LCB at Γ and the second LCB at M3 continue to decline, keeping HVB at Γ as the top of the valence band. This pressure dependence of the levels leads to a noticeable increase of the energy gap. From 1.5 to 2.0 GPa, both LCB at Γ and the second LCB at M3 begin to go up. On the other hand, it can be seen that LCB at Γ moves more slowly than the first LCB at M3. Consequently, the energy gap becomes direct and entirely

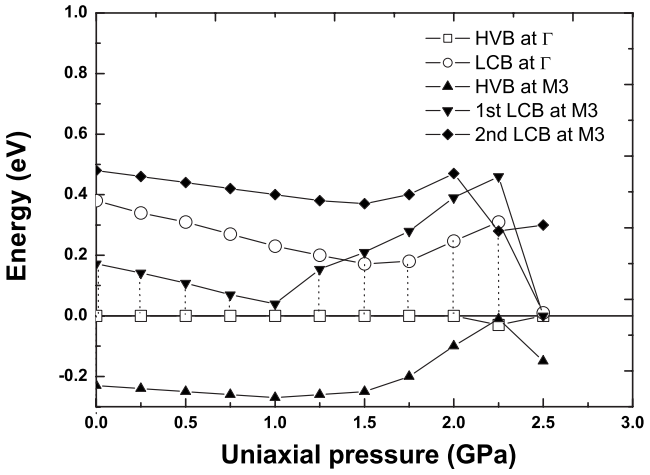

FIG. 12. Calculated pressure dependence of energy bands for the lowest conduction band (LCB) and the highest valence band (HVB) at the M3 and Γ points of the (10, 0) bundle. The top of the valence band on the Fermi level E_F is set to zero.

dependent on the band structure at the Γ point during this pressure range. Between 2.0 and 2.5 GPa, it seems by inspection of the dispersion relation that the characters of the "actual" first LCB and the "actual" second LCB at M3 exchange each other. Thus, we plotted the energy levels as crosses in Fig. 12. Under the pressure of 2.25 GPa, the first LCB at M3 and LCB at Γ become a peak. HVBs at the M3 and Γ points are slightly lower than the top of the valence band. In this case, the second LCB at M3 turns to be the actual lowest conduction band instead of the first LCB at M3, and the top of the valence band is at the M1 point (not shown in Fig. 12). At 2.5 GPa, the first LCB at M3 becomes the actual lowest conduction band again and meets with HVB at Γ on the Fermi level, then the energy gap of the bundle closes.

It has been indicated by the experiment[4] that the energy gap of the semiconducting bundle increases with increasing hydrostatic pressure and a structural transition could lead to a sudden drop in the energy gap. These results and suggestions are different from our results possibly because the applied pressure is hydrostatic in the experiment. A circular-to-elliptical shape transition is generated by the uniaxial pressure in the present work. Furthermore, the diameter of the SWCNTs used in the experiment is 14 Å and the diameter of the (10, 0) tube is 7.83 Å. The difference of pressure will make different manners in the deformation especially in the configuration of the carbon nanotubes. By considering the softness of the larger nanotubes, the difference in the diameter will also induce different configurations. This could make different band structures. Especially, our present work exhibited more complicated energy gap variations in the (10, 0) bundle.

D. Wave functions

In order to obtain a more detailed mechanism for the energy gap variation of the (10,0) bundle under pressure, we further investigated the electronic states in terms of the wave functions.

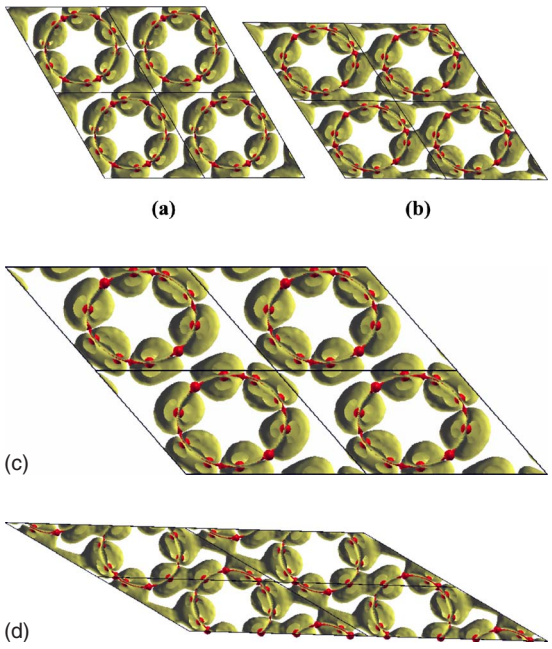

FIG. 13. (Color online) Equivalue plots of the wave function amplitude of LCB at M3 of the (10, 0) bundle under pressure at (a) 0 GPa ($e'=0.26$), (b) 1.0 GPa ($e'=0.47$), (c) 2.25 GPa ($e=0.52$), and (d) 2.5 GPa ($e'=0.62$). The gray surface (yellow online) is plotted for the absolute value 0.15 of the wave function normalized in the unit cell. The dark spheres (red online) represent the carbon atoms.

The energy gap variation of the (10, 0) bundle can be attributed mainly to the change of the conduction band, as described above. Figure 13 shows the wave function amplitude of LCB at M3 under (a) 0 GPa, (b) 1.0 GPa, (c) 2.25 GPa, and (d) 2.5 GPa. In Fig. 13(a), the wave function inside the nanotube is distributed mainly along the circumferential direction at 0 GPa with six nodes, corresponding to the lowest unoccupied molecular orbital of an isolated nanotube. However, the wave function distribution outside the tube shows a large difference from the inside. They are connected in the region along the short diagonal direction in the parallelogram of the unit cell (60° in the Cartesian x-y coordinate system), which would make a bonding orbital with the neighboring tubes. Along the x axis and the 120° direction in the x-y coordinate system, on the other hand, the wave function has a small amplitude outside the tube, indicating an antibonding orbital.

In Fig. 13(b), the shape of the wave function outside the nanotube is clearly changed, while the inside still keeps a similar shape as in Fig. 13(a). Under the pressure of 1.0 GPa, it is obvious, as shown in Fig. 13(b), that the outside wave functions are connected with those of its nearest neighbors in a different manner. In addition, it should be mentioned that the uniaxial pressure can induce the increase of the intertubular distance along the x axis and the decrease along the y axis. As a result, the intertubular atoms are forced to be closer to each other along the y axis.

At 2.25 GPa, shown in Fig. 13(c), the outside wave function shows no connection, having a flat surface facing each other between the tubes. This distribution of the outside wave function is completely different from those in given Figs. 13(a) and 13(b). If it is possible for the electrons to be on the outside wave functions, the intertubular atoms would have a complete antibonding interaction. At this pressure, the band structure of the bundle becomes more complicated and the energy gap of the bundle reaches its maximum.

At 2.5 GPa, the characteristics of the outside wave function become very prominent. Compared with Fig. 13(c), it is shown in Fig. 13(d) that the deformation in the geometry becomes larger and the shape of the outside wave function exhibits an abrupt change. The wave function distribution forms the connection between the tubes again. Under this pressure, the change of the wave function is large enough to induce a drop of the lowest conduction band and the disappearance of the energy gap.

Under pressure, a rotation of the nanotube can also be found in the deformed geometries, as shown in Fig. 13, in addition to symmetry lowering. We define the orientational angle Φ of an atom in a nanotube of the (10, 0) bundle, as indicated in Fig. 14(a). $\Delta\Phi$ is the angle difference between Φ of an atom at a certain pressure and that at 0 GPa. Figure 14(c) shows the variations of the angle difference $\Delta\Phi$ for different atoms [whose positions in one of the planes of the unit cell are shown in Fig. 14(b)] with pressure. Because the atoms were rotated in the same direction, for clear visibility, the sign of $\Delta\Phi$ is defined as negative if the atom is in the upper half of the tube, as shown in Fig. 14(b), and positive if the atom is in the lower half. In this case, it can be imagined that the nanotube is rotated clockwise, although different atoms are rotated by different angles at a certain pressure. The atoms move in such a way that each atom moves away from the others in the adjacent nanotubes, which might accompany the changes in the bond lengths and angles in the nanotube. The behaviors of $\Delta\Phi$ exhibit a strong dependence on atoms, such as oscillating for the C1 atom and monotonous decrease for the C7 atom in the upper half of the nanotube. However, the common feature is that the change rates of $\Delta\Phi$ are both very small from 1.25 to 2.25 GPa, during which the energy gap of the bundle would increase with pressure. For the curves given in Fig. 14(c), therefore, it can be approximately divided into three stages: (1) small rotations (0–1.25 GPa), (2) almost no rotation (1.25–2.25 GPa), and (3) large rotations (2.25–3.5 GPa). From a comparison with the energy gap change, we can see that the rotation of the nanotube plays a very important role in the changes of the electronic properties of the carbon nanotube bundle.

The theoretical band structure of the (10, 0) bundle was reported by Reich *et al.*[36] Their result indicated that the (10, 0) bundle is metallic at the ambient condition, although our present calculations gave us a finite energy gap. Considering the fact that the rotation of the nanotube is quite essential in the band structure at least for the (10, 0) bundle, the difference in the results may come from different configurations of the nanotubes employed in each case.

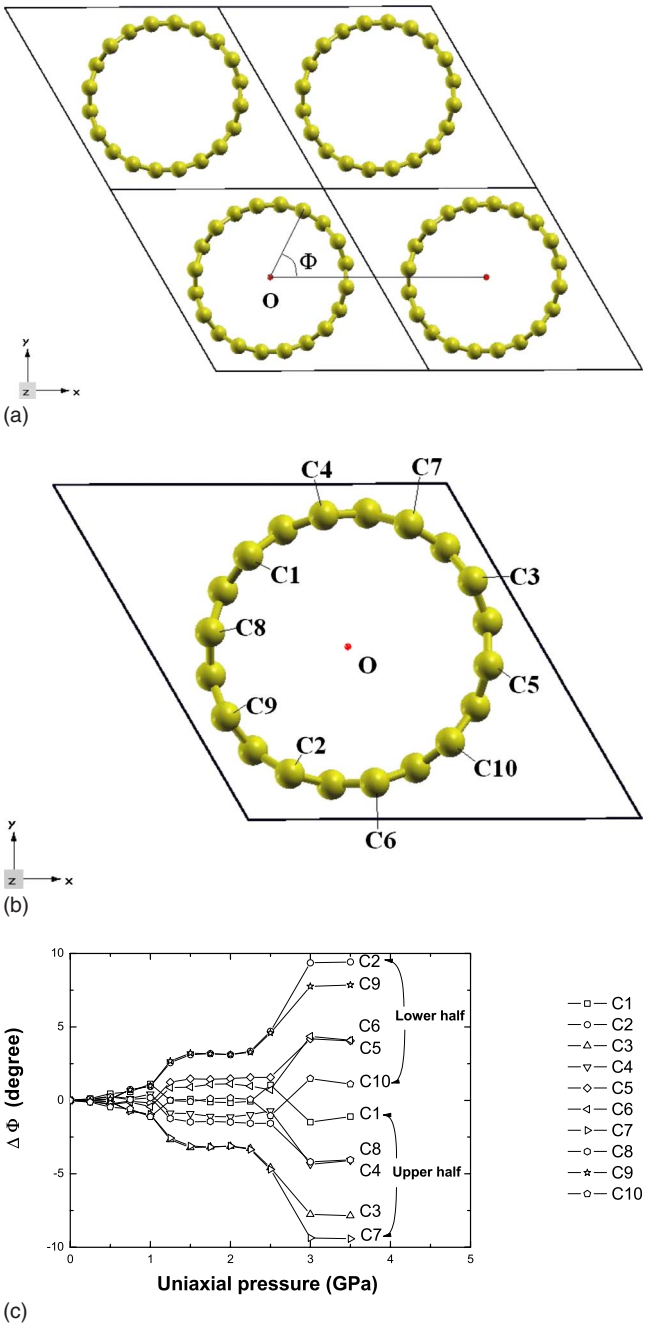

FIG. 14. (Color online) (a) Definition of the atomic orientational angle Φ for a tube in the (10, 0) bundle, (b) schematic view of atomic positions in one of the planes of the unit cell, and (c) variations of the angle difference $\Delta\Phi$ for different atoms as a function of pressure. The gray spheres (yellow online) in (a) and (b) represent carbon atoms.

IV. DISCUSSIONS AND CONCLUDING REMARKS

The changes in electronic structure induced by deformation have been investigated much for an isolated carbon nanotube.[23,38] The present study, however, has shown that changes of the configuration of the nanotubes have a stronger influence on the electronic properties of nanotube bundles. In some cases, noticeable deformation of the nanotubes such as structural collapses occurs in the metallic phase.

Elliot *et al.*[12] have reported a simple relation between the collapse pressure and the diameter of the tube forming a bundle on the basis of classical molecular dynamics simula-

tions for bundles of various types of the carbon nanotubes under hydrostatic pressure. On the contrary to their findings, the present calculations have shown a rather complicated behavior: the (8, 0), (10, 0), and (11, 0) bundles exhibit large deformation at uniaxial pressures of about 4, 2, and 6.5 GPa, respectively. Of course, the pressure conditions are different in the two studies. Moreover, since the present calculations suggested the change in the bonding between nanotubes when the nanotubes are deformed, further investigations, especially on the interactions between the deformed nanotubes, may be required to understand the discrepancies.

We have studied the effects of uniaxial pressure on the geometric structure and the electronic structure of the (8, 0), (10, 0), and (11, 0) SWCNT bundles by using the local-density approximation in the density-functional theory. The calculations have revealed a close relationship between the electronic structure of the bundle and its geometric changes. The lattice constants and the energy gap of the (8, 0) and (11, 0) bundles change similarly. However, there are some differences in the atomistic geometry after the deformation. While the (8, 0) bundle has the closely packed arrangement of the elliptic nanotubes, the (11, 0) bundle exhibits a loose configuration of the peanut-shaped nanotubes under high pressure. For the (10, 0) bundle, the pressure effect on the energy gap is rather complicated. After an initial decrease, the energy gap increases remarkably before metallization takes place, which has a different pressure dependence from that of the (8, 0) and (11, 0) bundles. However, in relation to the geometric and electronic structures of the bundles, they still have three common characteristics in the whole uniaxial pressure range: (1) semiconducting feature, (2) metallic character, and (3) large structural deformation.

By analyzing the band structure and wave functions, the essence of the variation of the electronic properties in the bundles can be revealed, especially from the beginning of applying pressure up to the semiconductor-metal transition. As a general trend of the band structure variation, the amplitude of change of the conduction band is substantially larger than that of the valence band in the electronic structure. Our calculations have shown that the change of the energy gap in the (11, 0) bundle is similar to that in the (8, 0) one. A common feature among the band structures of the (8, 0), (11, 0), and (10, 0) bundles is that the variations of the energy gap are primarily determined by the band structures at the M and Γ points. In the band structure of the (10, 0) bundle, the nature of the wave functions at the M3 point would play an important role. From the detailed analyses, it was found that the structural changes clearly affect the wave functions of the conduction band at the intertubular region. Accompanying the symmetry lowering of the carbon nanotube under pressure, tube rotation can also be found in the deformed geometries in the bundle which may significantly influence the electronic properties of the bundle. Therefore, the details about the effects of the deformation on the electronic structures of the SWCNT bundles cannot be described simply by a common calculation model.

ACKNOWLEDGMENTS

This work is partly supported by the Ministry of Education, Culture, Sports, Science and Technology in Japan, KAKENHI, No. 17064016. The calculations have been performed on the Numerical Materials Simulator (HITACHI SR11000) at the National Institute for Materials Science.

APPENDIX

Generally, the eccentricity e of an ellipse measures how far the ellipse deviates from a circle and is defined as $e=\sqrt{1-S^2/L^2}$, where S and L are the minor and major axes, respectively. In the SWCNT bundle, under the uniaxial pressure, a cross section of the (8, 0), (10, 0) and (11, 0) tubes is deformed almost elliptically to the tube diameter combined with the lattice constants a and b of the unit cell. However, the deformation in the actual tubes can be rather a peanut shape than a simple ellipse, as can be seen in Fig. 7(c). Thus, we define the eccentricity of the deformed tube as $e'=\sqrt{1-s^2/l^2}$, where $s=\mathrm{Min}_i|x_i-x_o|$ and $l=\mathrm{Max}_i|x_i-x_o|$ by using the two-dimensional coordinate of the ith atom x_i and that of the center of mass x_o on the xy plane.

[1] S. Iijima, Nature (London) **354**, 56 (1991).
[2] N. Hamada, S. I. Sawada, and A. Oshiyama, Phys. Rev. Lett. **68**, 1579 (1992).
[3] R. Saito, M. Fujita, G. Dresselhaus, and M. S. Dresselhaus, Appl. Phys. Lett. **60**, 2204 (1992).
[4] J. Tang, L. C. Qin, T. Sasaki, M. Yudasaka, A. Matsushita, and S. Iijima, J. Phys.: Condens. Matter **14**, 10575 (2002).
[5] C. W. Chen, M. H. Lee, and S. J. Clark, Nanotechnology **15**, 1837 (2004).
[6] S. H. Jhi, S. G. Louie, and M. L. Cohen, Phys. Rev. Lett. **95**, 226403 (2005).
[7] J. Tang, L. C. Qin, T. Sasaki, M. Yudasaka, A. Matsushita, and S. Iijima, Phys. Rev. Lett. **85**, 1887 (2000).
[8] S. M. Sharma, S. Karmakar, S. K. Sikka, P. V. Teredesai, A. K. Sood, A. Govindaraj, and C. N. R. Rao, Phys. Rev. B **63**, 205417 (2001).
[9] U. D. Venkateswaran, A. M. Rao, E. Richter, M. Menon, A. Rinzler, R. E. Smalley, and P. C. Eklund, Phys. Rev. B **59**, 10928 (1999).
[10] M. J. Peters, L. E. McNeil, J. P. Lu, and D. Kahn, Phys. Rev. B **61**, 5939 (2000).
[11] S. A. Chesnokov, V. A. Nalimova, A. G. Rinzler, R. E. Smalley, and J. E. Fischer, Phys. Rev. Lett. **82**, 343 (1999).
[12] J. A. Elliott, J. K. W. Sandler, A. H. Windle, R. J. Young, and M. S. P. Shaffer, Phys. Rev. Lett. **92**, 095501 (2004).
[13] M. J. López, A. Rubio, J. A. Alonso, L. C. Qin, and S. Iijima, Phys. Rev. Lett. **86**, 3056 (2001).
[14] S. Rols, I. N. Gontcharenko, R. Almairac, J. L. Sauvajol, and I. Mirebeau, Phys. Rev. B **64**, 153401 (2001).
[15] M. H. F. Sluiter, V. Kumar, and Y. Kawazoe, Phys. Rev. B **65**,

161402(R) (2002).
[16] X. H. Zhang, D. Y. Sun, Z. F. Liu, and X. G. Gong, Phys. Rev. B **70**, 035422 (2004).
[17] S. P. Chan, W. L. Yim, X. G. Gong, and Z. F. Liu, Phys. Rev. B **68**, 075404 (2003).
[18] O. Gülseren, T. Yildirim, and S. Ciraci, Phys. Rev. B **65**, 153405 (2002).
[19] G. Sun, J. Kürti, M. Kertesz, and R. H. Baughman, J. Phys. Chem. B **107**, 6924 (2003).
[20] V. Zólyomi and J. Kürti, Phys. Rev. B **70**, 085403 (2004).
[21] B. Kozinsky and N. Marzari, Phys. Rev. Lett. **96**, 166801 (2006).
[22] J. Akola, K. Rytkönen, and M. Manninen, J. Phys. Chem. B **110**, 5186 (2006).
[23] C. Kilic, S. Ciraci, O. Gülseren, and T. Yildirim, Phys. Rev. B **62**, R16345 (2000).
[24] D. Y. Sun, D. J. Shu, M. Ji, F. Liu, M. Wang, and X. G. Gong, Phys. Rev. B **70**, 165417 (2004).
[25] V. Gadagkar, P. K. Maiti, Y. Lansac, A. Jagota, and A. K. Sood, Phys. Rev. B **73**, 085402 (2006).
[26] A. Rochefort, D. R. Salahub, and Ph. Avouris, Chem. Phys. Lett. **297**, 45 (1998).
[27] T. Hertel, R. E. Walkup, and P. Avouris, Phys. Rev. B **58**, 13870 (1998).
[28] L. Kleinman and D. M. Bylander, Phys. Rev. Lett. **48**, 1425 (1982).
[29] N. Troullier and J. L. Martins, Phys. Rev. B **43**, 1993 (1991).
[30] X. Gonze, J. M. Beuken, R. Caracas, F. Detraux, M. Fuchs, G. M. Rignanese, L. Sindic, M. Verstraete, G. Zerah, F. Jollet, M. Terrent, A. Roy, M. Mikami, P. Ghosez, J. Y. Raty, and C. D. Allan, Comput. Mater. Sci. **25**, 478 (2002).
[31] D. M. Ceperley and B. J. Alder, Phys. Rev. Lett. **45**, 566 (1980).
[32] J. P. Perdew and Y. Wang, Phys. Rev. B **45**, 13244 (1992).
[33] M. C. Payne, M. P. Teter, D. C. Allan, T. A. Arias, and J. D. Joannopoulos, Rev. Mod. Phys. **64**, 1045 (1992).
[34] X. Gonze, Phys. Rev. B **54**, 4383 (1996).
[35] H. J. Monkhorst and J. D. Pack, Phys. Rev. B **13**, 5188 (1976).
[36] S. Reich, C. Thomsen, and P. Ordejón, Phys. Rev. B **65**, 155411 (2002).
[37] U. D. Venkateswaran, D. L. Masica, G. U. Sumanasekara, C. A. Furtado, U. J. Kim, and P. C. Eklund, Phys. Rev. B **68**, 241406(R) (2003).
[38] C.-J. Park, Y.-H. Kim, and K. J. Chang, Phys. Rev. B **60**, 10656 (1999).